JACS Au
AN OPEN ACCESS JOURNAL OF THE AMERICAN CHEMICAL SOCIETY

Editors' Choice
Open Access

pubs.acs.org/jacsau
Letter

Asparagusic Golgi Trackers

Saidbakhrom Saidjalolov, Xiao-Xiao Chen, Julia Moreno, Michael Cognet, Luis Wong-Dilworth, Francesca Bottanelli, Naomi Sakai, and Stefan Matile*

Cite This: JACS Au 2024, 4, 3759−3765
Read Online

ACCESS | Metrics & More | Article Recommendations | Supporting Information

ABSTRACT: Thiol-mediated uptake (TMU) is thought to occur through dynamic covalent cascade exchange networks. Here we show that the cascade accounting for TMU of asparagusic acid derivatives (AspA) ends in the Golgi apparatus (G) and shifts from disulfide to thioester exchange with palmitoyl transferases as the final exchange partner. As a result, AspA combined with pH-sensitive fluoresceins, red-shifted silicon-rhodamines, or mechanosensitive flipper probes selectively labels the Golgi apparatus in fluorescence microscopy images in living and fixed cells. AspA Golgi trackers work without cellular engineering and excel with speed, simplicity, generality, and compatibility with G/ER and cis/trans discrimination, morphological changes, anterograde vesicular trafficking, and superresolution imaging by stimulated emission depletion microscopy. Golgi flippers in particular can image membrane order and tension in the Golgi and, if desired, at the plasma membrane during TMU.

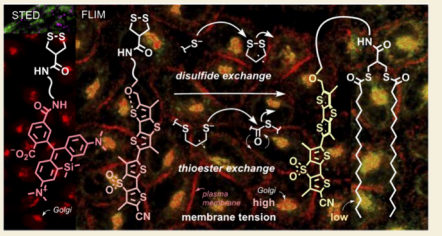

KEYWORDS: *Fluorescent probes, Golgi trackers, bioimaging, fluorescent flippers, cellular uptake, thiol-mediated uptake, palmitoylation*

Thiol-mediated uptake (TMU) is emerging as an enigmatic process that enables cellular entry of substrates appended with thiol-reactive moieties for drug delivery and drug discovery.[1−13] Efforts to decode the underlying thiol−disulfide exchange networks have focused on the identification of cellular exchange partners P_m that enable the penetration of the plasma membrane (PM) through toroidal elastics (Figure 1B, **I**−**III**).[1,2,14] In clear contrast, the intracellular partners P_i at the end of TMU cascades remain essentially unexplored. In this study, we show that derivatives of asparagusic acid[15] (AspA, **1**) accumulate in the Golgi apparatus to finish their thiol−disulfide-exchange-based TMU[1,2,14,16−19] as doubly palmitoylated amphiphiles like **2**, the products of dynamic covalent thioester exchange cascades[20−25] catalyzed by palmitoyl transferases (PATs)[26−32] as intracellular partners P_i (Figure 1B, **IV**−**VI**).

The specific labeling of intracellular sites of interest, organelles and beyond, is fundamental for bioimaging. Small-molecule trackers are particularly attractive because they can be added to living systems without genetic engineering or immunofluorescence procedures limited to fixed cells.[33−40] Most commercially available Golgi (G) trackers are sphingosine derivatives like **3** (Figure 2).[41−46] They generally suffer from complex and slow application protocols and limited selectivity, particularly with regard to G/ER discrimination.[42,43] Most recent progress with small-molecule Golgi trackers focused on cysteine derivatives.[42−54] For the Tsukiji probe **4**, palmitoylation by PATs in the Golgi has been demonstrated.[42]

Isosteric of singly palmitoylated AspA **5**, the Tsukiji probe **4** supported that palmitoylation could fix AspA-conjugates, e.g., **1** as a double-tail amphiphile **2** in the Golgi (Figure 2). Such probes could be advantageous for Golgi tracking because superb cellular uptake of AspA via thiol−disulfide exchange is well established,[1,2,14,16−19] while the two potentially precipitate-inducing greasy alkyl tails would be added only *in situ* at the site of interest (Figure 1B).

Asparagusates **1** and **6**−**8** were accessible from commercially available starting materials without extraordinary synthetic efforts (Figure 2, Schemes S1 and S2). Added to HK cells, FITC-AspA **6** (λ_{ex} 495 nm, λ_{em} 520 nm) labeled the Golgi in less than 10 min (Figure 3A; FITC: fluorescein thiourea). The brighter, red-shifted SiR-AspA **1** (Figure 3B, λ_{ex} 652 nm, λ_{em} 674 nm; SiR: silicon rhodamine[36,37,43,55,56]) and MaP555[57]-AspA **7** (Figures S8 and S10, λ_{ex} 555 nm, λ_{em} 580 nm) confirmed that Golgi tracking is fluorophore independent. The formation of hydrophobic palmitoylation products around[42] **2** and **5** could be detected in the HPLC of cell lysates (Figure 2B). The prepalmitoylated control **2** failed to label HK cells (Figure S11). This result confirmed the superiority of intracellular palmitoylation over prepalmitoylation for Golgi tracking (Figures 1B, 2).

Images obtained with SiR-AspA **1** were as good as those from immunofluorescence of Golgi proteins[58−62] (Figure 3C, D). However, immunofluorescence procedures require 3−5 h and work only in fixed cells, while Golgi tracking with SiR-

Received: June 7, 2024
Revised: July 29, 2024
Accepted: July 29, 2024
Published: August 20, 2024

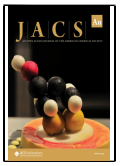

https://doi.org/10.1021/jacsau.4c00487
JACS Au 2024, 4, 3759−3765

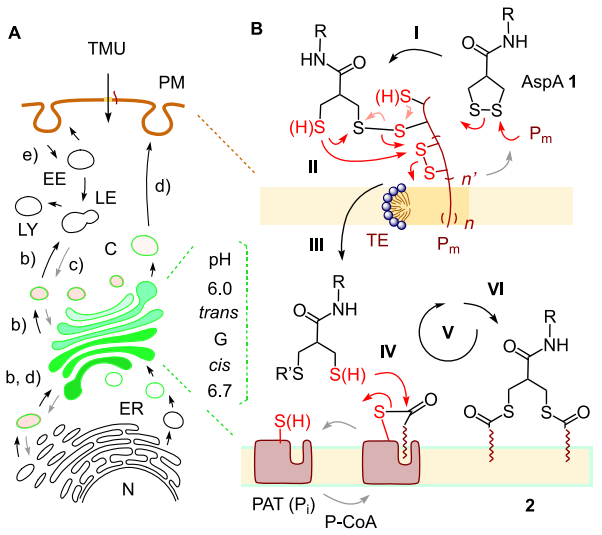

Figure 1. Thiol-mediated uptake, Golgi tracking, and vesicle trafficking. (A) Golgi apparatus (G) and vesicle trafficking, with endoplasmic reticulum (ER), nucleus (N), cytosol (C), lysosome (LY), late (LE) and early endosome (EE). (b) Anterograde and (c) retrograde transport (gray arrows), (d) secretory pathway, (e) endocytosis. (B) TMU of AspA **1** is found to end in the Golgi. Disulfide exchange cascades **I**–**III** with membrane-associated exchange partners (P_m) to cross the plasma membrane (PM) through toroidal elastics (TE) are terminated by thioester exchange **IV**–**VI** with palmitoyl transferases (PATs) as intracellular P_i.

AspA **1** takes 10 min and works also in living cells. Fixing of cells did not significantly affect brightness or location of AspA probes, consistent with their firm anchoring through palmitoylation (Figure S15).

As for established probes, Golgi tracking depended on probe concentration and incubation time (Figures S3–S10). At high concentrations, probes spread throughout the cells, probably due to oversaturation of the Golgi. FITC **6** was metabolized with $t_{50} \sim 1$ h as expected, while SiR **1** had a lifetime of $t_{50} \sim 4$ h (Figures S19, S20). AspA trackers were nontoxic (Figures S9, S10, S12, S16),[1,2,14,16−19] universal (e.g., HK, MCF-7, RPE-1, A431, MDCK cells, Figure S16), affected neither by ≤10% serum (Figure S14) nor by 500 μM cysteine (Figure S12), and ≥4 times enhanced by preincubation with BSA (Figure S13).

Automated comparison of masks (e.g., Figure 3H, I) for high-content (HC) imaging microscopy was applied to secure high-accuracy colocalization ratios (CoR), comparable to Pearson correlation coefficients (PCC). The PCC = 0.86 ± 0.02 (CoR = 0.87 ± 0.07) of AspA-SiR **1** against GM130 immunofluorescence was outstanding compared to known trackers (Figure 3B–D). Spreading into the ER, commercial trackers like **3** suffer from a Golgi to ER intensity ratio G/ER = 2.0.[42] G/ER = 6.0 of the Tsukiji probe **4** was considered a recent key breakthrough.[42] With AspA trackers, the ER was invisible (for **1**, G/ER > 20, PCC with ER tracker = 0.41 ± 0.02).

Most background fluorescence came from the cytosol. Incubation of 5 μM FITC-AspA **6** for 30 min gave a Golgi to cytosol ratio G/C = 8 (Figure 3K). For SiR **1** and MaP555 **7**, this further improved to G/C = 12. Control compounds, AspA dimers **8** and a simple cysteine[42−45,47−54] conjugate **9** were poor trackers with G/C < 4 (Figures 3K, 2, S4–S6). The previously reported GFP-AspA **10** did not track the Golgi (G/C ≪ 1).[18] This lost attraction to the Golgi could confirm that the envisioned traceless protein delivery by cytosolic esterolysis was indeed successful.[18]

Colocalization of SiR **1** with FITC **6** was poor (CoR = 0.67, Figure 3E). This implied that **6** could selectively track *cis* Golgi (pH = 6.7) because the pH-sensitive FITC (pK_a = 6.4) is quenched in *trans* Golgi (pH = 6.0, Figure 1A) if a significant portion of the Golgi trackers faces toward the Golgi lumen, possibly implying flip-flop. Although difficult to prove, this interpretation was supported empirically by the similarly poor colocalization of *cis*/*median*-selective immunofluorescent antibody GM130,[58,59,62] against the *trans*-selective TGN46 (CoR = 0.74, Figure 3H),[60,61] and of **6** (*cis*) against TGN46 (*trans*, 0.69, Figure 3F), and also by the good colocalization of **6** (*cis*)

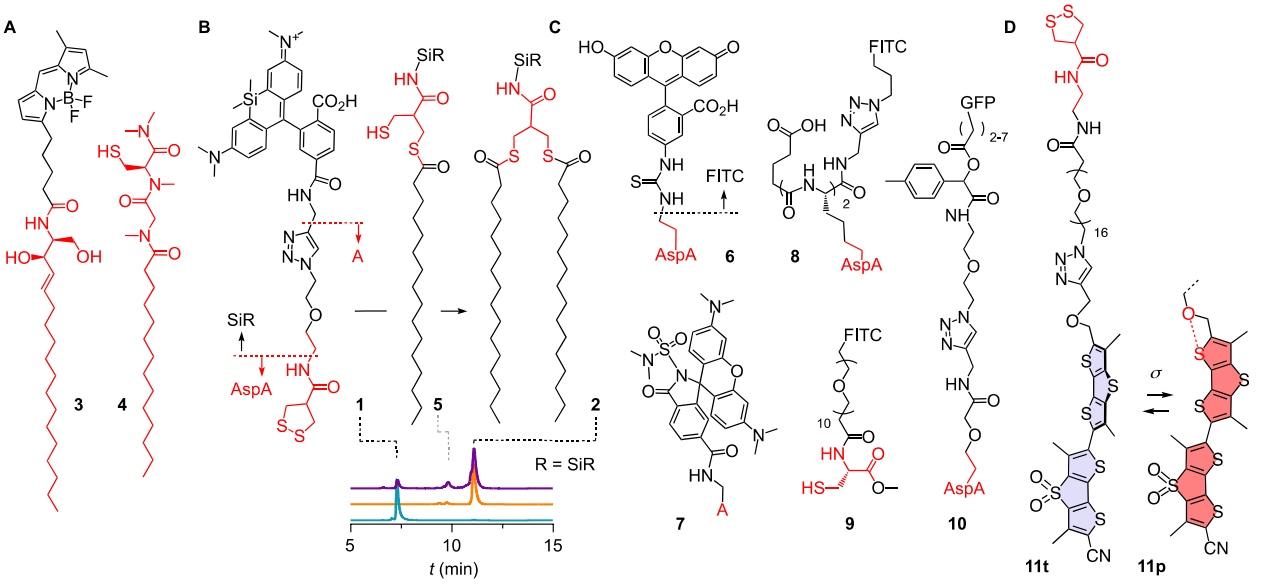

Figure 2. Structure and function of Golgi trackers. (A) Representative existing Golgi trackers. (B) SiR-AspA **1** with palmitoylation products **5** and **2** and HPLC traces of cell extracts (top) compared to pure **2** (middle) and **1** (bottom). (C) FITC-AspA **6** and controls (GFP = green fluorescent protein). (D) Golgi-Flipper **11**, with compression of twisted **11t** into planar **11p** by physical forces σ.

https://doi.org/10.1021/jacsau.4c00487
JACS Au 2024, 4, 3759−3765

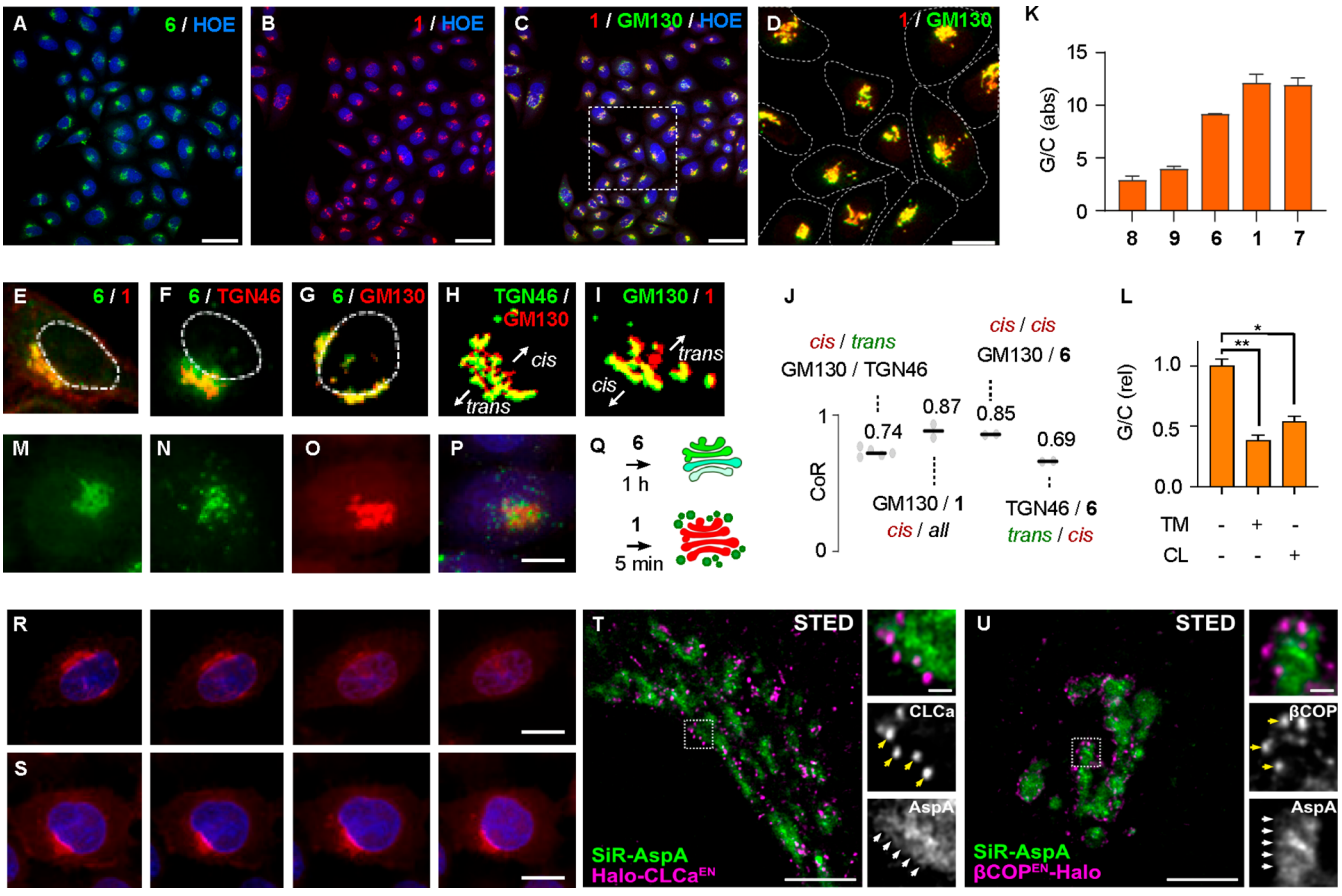

Figure 3. Evaluation of Golgi trackers. (A–G) SDCM images of fixed HK cells with (A) **6**, (B, C) **1**, (C) **1** and GM130, (D) zoom of (C) with cell boundaries (white dashed), (E) **6** (green, *cis*) and **1** (red, *all*), (F) **6** (green, *cis*) and TGN46 (red, *trans*), (G) **6** (green, *cis*) and GM130 (red, *cis-median*) with nuclei boundaries (E–G, white dashed), (H, I) masks generated for (H) GM130 (red, *cis-median*) and TGN46 (green, *trans*), and (I) GM130 (green, *cis-median*) and **1** (red, *all*). (J) Colocalization ratios for (F–I). (K, L) Golgi/cytosol (G/C) ratios for (K) **1**, **6**–**9** and for (L) **1** treated with tunicamycin (TM) and cerulenin (CL). (M–Q) SDCM images of live HK cells for sequential tracking (Q) with **6** (green, 20 μM) for (M) 1 h, then (N) 5 min after the addition of (O) **1** (red, 500 nM, (P) = (N) + (O) merged). (R, S) SDCM images of live HK cells with **1** with (R) and without (S) brefeldin A for 0, 10, 30, 60 min (from left). (T, U) Live-cell STED images of HeLa cells with **1** (green) expressing endogenously tagged (T) $CLCa^{EN}$-Halo and (U) βCOP^{EN}-Halo labeled with JF_{571}–CA (magenta). Blue: Hoechst 33342 (HOE), scale bars: 50 μm (A–C), 20 μm (D), 10 μm (M–S), 5 and 0.5 μm in the crops (T, U).

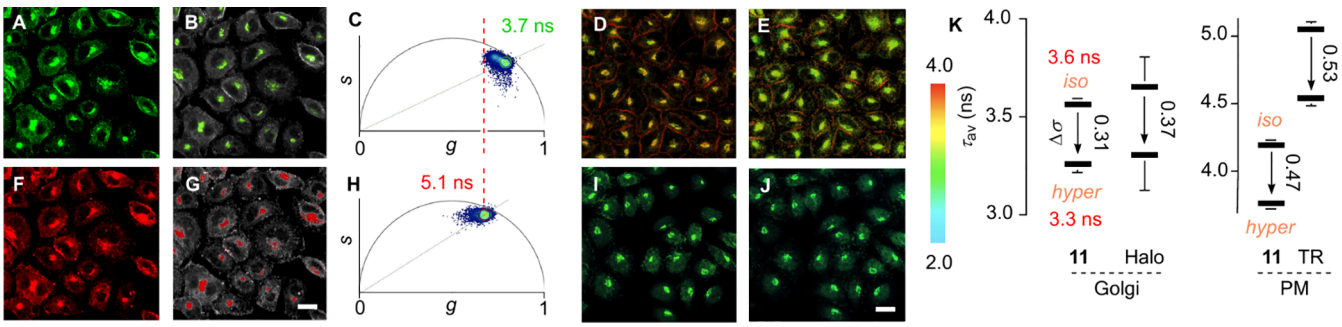

Figure 4. Golgi flippers. Comparison of HK cells with either **11** (A–E, λ_{ex} = 480 nm, detection 600–650 nm), **3** (F–H, λ_{ex} = 480 nm, detection 510–540 nm), or **1** (I, J, λ_{ex} = 600 nm, detection 630–800 nm) in (A, F) CLSM images, (B, G) FLIM images reconstructed from their (C, H) phasor hemispheres, (D, I) FLIM images under isoosmotic and (E, J) hyperosmotic conditions; scale bars: 20 μm. (K) Lifetimes and changes from isoosmotic to hyperosmotic HK cells (arrows, $\Delta\sigma$) for **11** in Golgi compared to HaloFlippers in Golgi and **11** in PM compared to Flipper-TR.

with the less selective GM130 (*cis-median*, 0.85, Figure 3G) and GM130 with the less selective **1** (*all*, 0.87, Figure 3I).

Live-cell stimulated emission depletion (STED) images of SiR-AspA **1** confirmed compatibility of this new Golgi tracker with multicolor superresolution microscopy (Figure 3T, U).[62,63] Labeling of cells expressing endogenously Halo-tagged clathrin (Halo-$CLCa^{EN}$, EN = endogenous) and COPI ($BetaCOP^{EN}$-Halo)[63] showed that AspA **1** tracks both *cis* and *trans* Golgi and defines Golgi cisternae decorated by coat proteins at their rims/edges (Figures 3T, U; 1b, c).[63]

SiR-AspA **1** faithfully showed the morphological changes of the Golgi caused by brefeldin A[64] (Figure 3R, S). With AspA **6**

https://doi.org/10.1021/jacsau.4c00487
JACS Au 2024, 4, 3759–3765

at higher concentrations, labeling changed within 1 h from the Golgi to clustered puncta spreading from the Golgi, as evidenced by pulse-chase type tracking after the addition (chase) of AspA **1** at low concentrations (Figure 3M−Q). Thus, at higher concentrations (low micromolar) and after a longer incubation time (∼1 h), AspA trackers report on anterograde vesicular trafficking from the Golgi to endo/lysosomes but not to the PM (Figure 1A, b). This differed from lower concentrations (nanomolar), where AspA trackers reported from the Golgi membrane for hours without change (Figure 3S). Since palmitoylation is involved in anterograde transport (Figure 1A, b),[27] these findings supported that Golgi tracking by AspA operates indeed by dynamic covalent thioester exchange (Figures 1, 2). Further support for operational palmitoylation of AspA in the Golgi could be obtained with PAT inhibitors tunicamycin (TM)[65] and cerulenin (CL).[66] The G/C ratio of **1** decreased in their presence, with the former by more than 50% (Figure 3L).

Fluorescent flippers have been introduced over the past decade as small molecule probes to image physical forces, that is, membrane tension, in living systems.[40,67−70] To explore AspA trackers for flipper research, Golgi flipper **11** was synthesized (Scheme S3). While emission from the Golgi was qualitatively obvious, colocalization of **11** with **3** was technically challenging by confocal laser scanning microscopy (CLSM) because of bleed-through fluorescence (Figure 4A, F). However, in fluorescence lifetime imaging microscopy (FLIM) phasor hemispheres,[71−73] τ = 3.7 ns of flipper **11** appeared well separated from τ = 5.1 ns of BODIPY **3** (Figure 4C, H). FLIM images mapped from the phasor hemispheres for HK cells labeled with both probes localized the origin of both lifetime maxima in the Golgi (Figures 4B, G).

Physical compression of the favored twisted conformer **11t** into the planar conformer **11p** reports an increase in membrane order or tension with red-shifted emission and longer lifetimes (Figure 2).[40,67−69,74,75] Under hyperosmotic stress, the lifetime of **11** in the Golgi decreased from τ_{av} = 3.6 ns by $\Delta\tau_{av}$ = −0.3 ns to τ_{av} = 3.3 ns (Figure 4D, E, K). Lifetime and response to reduced membrane tension were in the range of Halo-Flippers attached to sialyltransferases in the Golgi by genetic engineering (Figure 4K, Halo).[76] As expected, SiR-AspA **1** was insensitive to changes in membrane tension ($\Delta\tau_{av}$ < 0.1 ns, Figure 4I, J).

Flippers **11** were partially retained in the plasma membrane (PM, Figure 4D, E), unlike hydrophilic probes like FITC or SiR (Figure 3A-D). This suggested that hydrophobically matching fluorophores like flippers could partially interrupt TMU at the PM and remain attached to the transferrin receptor[14] or other P_m (Figure 1).[2] The τ_{av} = 4.2 ns of **11** in the PM (Figure 4D, K) was shorter than the τ_{av} = 5.1 ns of the original Flipper TR[74,77] (Figure 4K). These differences at preserved responsiveness to tension (Figure 4E, K) suggested that the local membrane environment of P_m during TMU could be less ordered than the rest of the PM. Transporter-flipper conjugates could thus possibly provide insights on local changes in membrane architecture during TMU, including toroidal elastics (Figure 1).[2]

In summary, this study identifies palmitoyl transferases in the Golgi as final partners in the exchange cascades that account for TMU of asparagusates, thus ending up with a shift from disulfide to dynamic covalent thioester exchange. Established early on as unique monomers to directionally grow functional dynamer surface architectures[78−80] and to open up new entries into cells,[1,16] their emergence as Golgi trackers endorses the asparagusic acid motif[15] as a truly privileged scaffold, tiny but full of positive surprises.

METHODS

Tracker Synthesis

To a solution of the NHS-ester of asparagusic acid[16] (150 mg, 607 μmol, **12**) in dry CH_2Cl_2 (50 mL) was added 2-(2-azidoethoxy)ethan-1-amine[81] (152 mg, 910 μmol, HCl salt, **13**) and DIPEA (429 μL, 2.43 mmol). The reaction mixture was stirred at rt overnight. Then it was quenched with 1 M HCl. The crude product was extracted with CH_2Cl_2 (x3), washed with brine, dried over Na_2SO_4 and concentrated *in vacuo*. The crude product was subjected to purification by flash chromatography (Scorpius silica 12 g, CH_2Cl_2/MeOH 95:5) to afford the desired amide (155 mg, 97%, **14**) as a colorless solid. R_f (CH_2Cl_2/MeOH 95:5): 0.52; Mp: 54−55 °C; IR (neat): 3296 (br, NH), 2101 (s, N_3), 1637 (s, C═O), 1551 (s, N−C═O), 1297 (m), 1250 (s), 1112 (s, C−O−C), 1079 (s, C−O−C), 1045 (m, C−O), 683 (s, C−S); ^{1}H NMR (400 MHz, $CDCl_3$): 6.17 (s, 1H), 3.70 (t, $^3J_{H-H}$ = 4.0 Hz, 2H), 3.58 (t, $^3J_{H-H}$ = 5.0 Hz, 2H), 3.51 (q, $^3J_{H-H}$ = 5.0 Hz, 2H), 3.40−3.37 (m, 4H), 3.36 (s, 2H), 3.16 (p, $^3J_{H-H}$ = 7.0 Hz, 1H); ^{13}C NMR (126 MHz, $CDCl_3$): 171.8 (C), 70.4 (CH_2), 69.8 (CH_2), 52.6 (CH), 50.8 (CH_2), 42.8 ($2CH_2$), 39.6 (CH_2); LRMS (ESI): 263 ($C_8H_{15}N_4O_2S_2$, [M + H]$^+$).

To a mixture of azide **14** (7.2 mg, 28 μmol) and alkyne **15** (7.0 mg, 14 μmol) in dry THF (5.0 mL) under N_2 atmosphere was added a premixed solution of CuI (5.2 mg, 28 μmol) and THPTA (6.0 mg, 14 μmol) in dry THF. The reaction mixture was stirred at rt for 30 h (completion evidenced by LC-MS). The crude mixture was filtered to remove the excess of CuI and then the filtrate was concentrated *in vacuo*. RP-chromatography (Scorpius C18 33g, H_2O + 0.1% TFA/CH_3CN + 0.1% TFA, 1:1) afforded **1** (4.7 mg, 44%) as a blue solid. Mp: 120−121 °C; IR (neat): 2923 (br, NH), 1658 (s, C═O), 1575 (s, N−C═O), 1353 (s, C−N), 1314 (s, C−N), 1124 (s, $Si(CH_3)_2$), 922 (w, CH), 835 (m, Si−C), 719 (w); ^{1}H NMR (500 MHz, DMSO-d_6): 9.30 (t, $^3J_{H-H}$ = 5.7 Hz, 1H), 8.16−8.08 (m, 2H), 8.04 (d, $^3J_{H-H}$ = 8.0 Hz, 1H), 7.94 (s, 1H), 7.72 (s, 1H), 7.04 (s, 2H), 6.76−6.51 (m, 4H), 4.47−4.45 (m, 4H), 3.76 (t, $^3J_{H-H}$ = 5.3 Hz, 2H), 3.40 (t, $^3J_{H-H}$ = 5.7 Hz, 2H), 3.36−3.29 (m, 2H), 3.18 (q, $^3J_{H-H}$ = 5.7 Hz, 2H), 3.15−3.09 (m, 3H), 2.93 (s, 12H), 0.64 (s, 3H), 0.52 (s, 3H); ^{13}C NMR (126 MHz, DMSO-d_6): 170.5 (C), 169.2 (C), 164.7 (C), 158.2 (C), 154.7 (C), 149.2 (2C), 144.3 (C), 139.1 (C), 136.0 (2C), 130.5 (C), 128.3 (2CH), 127.7 (2CH), 125.4 (C), 123.5 (CH), 123.0 (CH), 116.5 (2CH), 113.9 (2CH), 91.3 (C), 68.6 (CH_2), 68.4 (CH_2), 51.3 (CH), 49.2 (CH_2), 42.1 ($2CH_2$), 40.0 ($4CH_3$), 38.7 (CH_2), 35.0 (CH_2), 0.0 (CH_3), −1.4 (CH_3); HRMS (ESI, + ve) calcd for $C_{38}H_{45}N_7O_5S_2Si$ [M + Na]$^+$: 794.2585, found: 794.2574.

Trackers other than SiR-AspA **1** were synthesized analogously, see Supporting Information.

Golgi Tracking

Human cervical cancer-derived HeLa Kyoto, human breast cancer-derived MCF-7, human retinal pigment epithelial-1 (RPE-1), Madin-Darby canine kidney (MDCK) and human epidermoid carcinoma (A-431) cells were cultured in complete FDMEM, i.e., FluoroBrite DMEM (GlutaMAX, 4.5 g/L D-glucose), supplemented with 10% fetal calf serum (FCS) and 1% Penicillin/Streptomycin (PS). HeLa CCL-2 (ECACC

https://doi.org/10.1021/jacsau.4c00487
JACS Au 2024, 4, 3759−3765

General Collection) were cultivated in DMEM supplemented with 10% FBS and 1% PS. The cells were grown under 5% CO_2 humidified atmosphere at 37 °C on a 75 cm^3 tissue culture flask (TPD Corporation). Cells were harvested by treatment with 3 mL of phenol-red free TrypLE Express, followed by the addition of 10 mL of complete FDMEM at 37 °C. The cells were spun down at 1500 g for 3 min, resuspended in complete FDMEM, and plated according to the concentration needed. For uptake or inhibition experiments, the cells were seeded in a μ-Plate 96-well Black ibiTreat sterile at 12 000 cells/well (HK, RPE-1, A-431) or 18 000 cells/well (MCF-7, MDCK) in complete FDMEM and left incubating under 5% CO_2 humidified atmosphere at 37 °C overnight.

From cells thus prepared in a 96 well plate, medium was removed, and cells were washed with PBS (3 × 3 mL/well) followed by fresh FDMEM serum-free medium (4 × 100 μL/well) using a plate washer (Biotek EL406), and kept in a 100 μL of the latter medium. Solutions of **1**, **2**, **6**−**9** (2−10 mM, DMSO) were diluted in FDMEM to give a solution at 3× final concentration, of which 50 μL was added to the well resulting in a final volume of 150 μL per well. The cells were incubated under 5% CO_2 humidified atmosphere at 37 °C for the indicated time (5−120 min). Then, the cells were washed with PBS (3 × 3 mL/well) and the medium was exchanged with FDMEM keeping a final volume of 100 μL/well, and a solution of Hoechst 33342 (100 μg/mL) in PBS (50 μL/well) was added. After 10 min of incubation under 5% CO_2 humidified atmosphere at 37 °C, cells were washed with PBS (3 × 3 mL/well) and kept in FDMEM (100 μL/well) for live cell imaging. For fixed cell imaging, the cells were treated with a solution of PFA 3% (70 μL/well) for 15 min at rt. The excess of PFA was removed by washing with PBS (9 × 3 mL/well). The distribution of fluorescent signals was captured on a IXM-C automated microscope with two channels, blue for Hoechst 33342 (377/50 nm excitation filter; 477/60 nm emission filter), and green (475/34 nm excitation filter; 536/40 nm emission filter, for **6**, **8**, and **9**), red (531/40 nm excitation filter; 593/40 nm emission filter, for **7**) or far red (620/50 nm; emission filter: 690/50 nm, for **1** or **2**). The rest of the parameters were adjusted according to the nature of the experiment. Duplicates were performed for each condition. The resulting images were automatically analyzed and quantified using the MetaXpress software.

■ ASSOCIATED CONTENT

Supporting Information

The Supporting Information is available free of charge at https://pubs.acs.org/doi/10.1021/jacsau.4c00487.

Detailed experimental procedures, materials and methods, synthesis, SDCM procedures, colocalization ratios from automated HC imaging, FLIM procedures, membrane tension measurement, original images (PDF)

■ AUTHOR INFORMATION

Corresponding Author

Stefan Matile − *Department of Organic Chemistry, University of Geneva, CH-1211 Geneva, Switzerland;* orcid.org/0000-0002-8537-8349; Email: stefan.matile@unige.ch

Authors

Saidbakhrom Saidjalolov − *Department of Organic Chemistry, University of Geneva, CH-1211 Geneva, Switzerland*

Xiao-Xiao Chen − *Department of Organic Chemistry, University of Geneva, CH-1211 Geneva, Switzerland*

Julia Moreno − *Department of Organic Chemistry, University of Geneva, CH-1211 Geneva, Switzerland*

Michael Cognet − *Department of Organic Chemistry, University of Geneva, CH-1211 Geneva, Switzerland;* orcid.org/0009-0000-1449-8979

Luis Wong-Dilworth − *Institute for Chemistry and Biochemistry, Freie Universität Berlin, D-14195 Berlin, Germany*

Francesca Bottanelli − *Institute for Chemistry and Biochemistry, Freie Universität Berlin, D-14195 Berlin, Germany*

Naomi Sakai − *Department of Organic Chemistry, University of Geneva, CH-1211 Geneva, Switzerland;* orcid.org/0000-0002-9460-1944

Complete contact information is available at: https://pubs.acs.org/10.1021/jacsau.4c00487

Notes

The authors declare the following competing financial interest(s): The University of Geneva has licensed Flipper-TR probes to Spirochrome for commercialization.

■ ACKNOWLEDGMENTS

We thank the NMR, MS, ACCESS and Bioimaging Platforms for services, L. Reymond, V. Mercier and D. Moreau for advise, Spirochrome for a gift of SiR and MaP555 dyes, and the University of Geneva, the National Centre of Competence in Research (NCCR) Molecular Systems Engineering (51NF40-205608), the Swiss NSF (Swiss-ERC Advanced Grant TIMEUP, TMAG-2_209190; Excellence Grant 200020 204175, all S.M.); the Freie Universität Berlin and the German Research Foundation (DFG, 278001972−TRR 186, all F. B.) for financial support.

■ REFERENCES

(1) Laurent, Q.; Martinent, R.; Lim, B.; Pham, A.-T.; Kato, T.; López-Andarias, J.; Sakai, N.; Matile, S. Thiol-Mediated Uptake. *JACS Au* **2021**, *1*, 710−728.

(2) Saidjalolov, S.; Coelho, F.; Mercier, V.; Moreau, D.; Matile, S. Inclusive Pattern Generation Protocols to Decode Thiol-Mediated Uptake. *ACS Cent. Sci.* **2024**, *10*, 1033−1043.

(3) Du, S.; Liew, S. S.; Li, L.; Yao, S. Q. Bypassing Endocytosis: Direct Cytosolic Delivery of Proteins. *J. Am. Chem. Soc.* **2018**, *140*, 15986−15996.

(4) Zhou, J.; Sun, L.; Wang, L.; Liu, Y.; Li, J.; Li, J.; Li, J.; Yang, H. Self-Assembled and Size-Controllable Oligonucleotide Nanospheres for Effective Antisense Gene Delivery through an Endocytosis-Independent Pathway. *Angew. Chem., Int. Ed.* **2019**, *58*, 5236−5240.

(5) Chen, Y.; Ping, Y. Development of CRISPR/Cas Delivery Systems for In Vivo Precision Genome Editing. *Acc. Chem. Res.* **2023**, *56*, 2185−2196.

(6) Ulrich, S. Growing Prospects of Dynamic Covalent Chemistry in Delivery Applications. *Acc. Chem. Res.* **2019**, *52*, 510−519.

(7) Shchelik, I. S.; Gademann, K. Synthesis and Antimicrobial Evaluation of New Cephalosporin Derivatives Containing Cyclic Disulfide Moieties. *ACS Infect. Dis.* **2022**, *8*, 2327−2338.

(8) Goerdeler, F.; Reuber, E. E.; Lühle, J.; Leichnitz, S.; Freitag, A.; Nedielkov, R.; Groza, R.; Ewers, H.; Möller, H. M.; Seeberger, P. H.;

Moscovitz, O. Thiol-Mediated Uptake of a Cysteine-Containing Nanobody for Anticancer Drug Delivery. *ACS Cent. Sci.* **2023**, *9*, 1111−1118.
(9) Mou, Q.; Xue, X.; Ma, Y.; Banik, M.; Garcia, V.; Guo, W.; Wang, J.; Song, T.; Chen, L.-Q.; Lu, Y. Efficient Delivery of a DNA Aptamer-Based Biosensor into Plant Cells for Glucose Sensing through Thiol-Mediated Uptake. *Sci. Adv.* **2022**, *8*, No. eabo0902.
(10) Shu, Z.; Tanaka, I.; Ota, A.; Fushihara, D.; Abe, N.; Kawaguchi, S.; Nakamoto, K.; Tomoike, F.; Tada, S.; Ito, Y.; Kimura, Y.; Abe, H. Disulfide-Unit Conjugation Enables Ultrafast Cytosolic Internalization of Antisense DNA and siRNA. *Angew. Chem., Int. Ed.* **2019**, *58*, 6611−6615.
(11) Meng, X.; Li, T.; Zhao, Y.; Wu, C. CXC-Mediated Cellular Uptake of Miniproteins: Forsaking "Arginine Magic. *ACS Chem. Biol.* **2018**, *13*, 3078−3086.
(12) Wan, Y.; Wang, W.; Lai, Q.; Wu, M.; Feng, S. Advances in Cell-Penetrating Poly(Disulfide)s for Intracellular Delivery of Therapeutics. *Drug Discovery Today* **2023**, *28*, No. 103668.
(13) Guo, J.; Chen, S.; Onishi, Y.; Shi, Q.; Song, Y.; Mei, H.; Chen, L.; Kool, E. T.; Zhu, R.-Y. RNA Control via Redox-Responsive Acylation. *Angew. Chem., Int. Ed.* **2024**, *63*, No. e202402178.
(14) Abegg, D.; Gasparini, G.; Hoch, D. G.; Shuster, A.; Bartolami, E.; Matile, S.; Adibekian, A. Strained Cyclic Disulfides Enable Cellular Uptake by Reacting with the Transferrin Receptor. *J. Am. Chem. Soc.* **2017**, *139*, 231−238.
(15) Ņikitjuka, A.; Žalubovskis, R. Asparagusic Acid − A Unique Approach toward Effective Cellular Uptake of Therapeutics: Application, Biological Targets, and Chemical Properties. *ChemMedChem.* **2023**, *18*, No. e202300143.
(16) Gasparini, G.; Sargsyan, G.; Bang, E.-K.; Sakai, N.; Matile, S. Ring Tension Applied to Thiol-Mediated Cellular Uptake. *Angew. Chem., Int. Ed.* **2015**, *54*, 7328−7331.
(17) Martinent, R.; Tawffik, S.; López-Andarias, J.; Moreau, D.; Laurent, Q.; Matile, S. Dithiolane Quartets: Thiol-Mediated Uptake Enables Cytosolic Delivery in Deep Tissue. *Chem. Sci.* **2021**, *12*, 13922−13929.
(18) Maynard, J. R. J.; Saidjalolov, S.; Velluz, M.-C.; Vossio, S.; Aumeier, C.; Moreau, D.; Sakai, N.; Matile, S. Toward a Traceless Tag for the Thiol-Mediated Uptake of Proteins. *ChemistryEurope* **2023**, *1*, No. e202300029.
(19) Tirla, A.; Rivera-Fuentes, P. Peptide Targeting of an Intracellular Receptor of the Secretory Pathway. *Biochemistry* **2019**, *58*, 1184−1187.
(20) Yuan, J.; Xiong, W.; Zhou, X.; Zhang, Y.; Shi, D.; Li, Z.; Lu, H. 4-Hydroxyproline-Derived Sustainable Polythioesters: Controlled Ring-Opening Polymerization, Complete Recyclability, and Facile Functionalization. *J. Am. Chem. Soc.* **2019**, *141*, 4928−4935.
(21) Woll, M. G.; Gellman, S. H. Backbone Thioester Exchange: A New Approach to Evaluating Higher Order Structural Stability in Polypeptides. *J. Am. Chem. Soc.* **2004**, *126*, 11172−11174.
(22) Ura, Y.; Al-Sayah, M.; Montenegro, J.; Beierle, J. M.; Leman, L. J.; Ghadiri, M. R. Dynamic Polythioesters Viaring-Opening Polymerization of 1,4-Thiazine-2,5-Diones. *Org. Biomol. Chem.* **2009**, *7*, 2878−2884.
(23) Mavila, S.; Worrell, B. T.; Culver, H. R.; Goldman, T. M.; Wang, C.; Lim, C.-H.; Domaille, D. W.; Pattanayak, S.; McBride, M. K.; Musgrave, C. B.; Bowman, C. N. Dynamic and Responsive DNA-like Polymers. *J. Am. Chem. Soc.* **2018**, *140*, 13594−13598.
(24) Kent, S. B. H. Total Chemical Synthesis of Proteins. *Chem. Soc. Rev.* **2009**, *38*, 338−351.
(25) Lim, B.; Sakai, N.; Matile, S. Tetrel-Centered Exchange Cascades to Decouple Inhibition and Induction of Thiol-Mediated Uptake: Introducing Cell-Penetrating Thiolactones, Focus on Reversible Michael Acceptor Dimers. *Helv. Chim. Acta* **2023**, *106*, No. e202300020.
(26) Jiang, H.; Zhang, X.; Chen, X.; Aramsangtienchai, P.; Tong, Z.; Lin, H. Protein Lipidation: Occurrence, Mechanisms, Biological Functions, and Enabling Technologies. *Chem. Rev.* **2018**, *118*, 919−988.
(27) Ernst, A. M.; Syed, S. A.; Zaki, O.; Bottanelli, F.; Zheng, H.; Hacke, M.; Xi, Z.; Rivera-Molina, F.; Graham, M.; Rebane, A. A.; Björkholm, P.; Baddeley, D.; Toomre, D.; Pincet, F.; Rothman, J. E. S-Palmitoylation Sorts Membrane Cargo for Anterograde Transport in the Golgi. *Dev. Cell* **2018**, *47*, 479−493.e7.
(28) Li, X.; Shen, L.; Xu, Z.; Liu, W.; Li, A.; Xu, J. Protein Palmitoylation Modification During Viral Infection and Detection Methods of Palmitoylated Proteins. *Front. Cell. Infect. Microbiol.* **2022**, *12*, No. 821596.
(29) Schulte-Zweckel, J.; Dwivedi, M.; Brockmeyer, A.; Janning, P.; Winter, R.; Triola, G. A Hydroxylamine Probe for Profiling S-Acylated Fatty Acids on Proteins. *Chem. Commun.* **2019**, *55*, 11183−11186.
(30) Philippe, J. M.; Jenkins, P. M. Spatial Organization of Palmitoyl Acyl Transferases Governs Substrate Localization and Function. *Mol. Membr. Biol.* **2019**, *35*, 60−75.
(31) Chavda, B.; Arnott, J. A.; Planey, S. L. Targeting Protein Palmitoylation: Selective Inhibitors and Implications in Disease. *Expert Opin. Drug Discovery* **2014**, *9*, 1005−1019.
(32) Hong, J. Y.; Malgapo, M. I. P.; Liu, Y.; Yang, M.; Zhu, C.; Zhang, X.; Tolbert, P.; Linder, M. E.; Lin, H. High-Throughput Enzyme Assay for Screening Inhibitors of the ZDHHC3/7/20 Acyltransferases. *ACS Chem. Biol.* **2021**, *16*, 1318−1324.
(33) Ma, J.; Sun, R.; Xia, K.; Xia, Q.; Liu, Y.; Zhang, X. Design and Application of Fluorescent Probes to Detect Cellular Physical Microenvironments. *Chem. Rev.* **2024**, *124*, 1738−1861.
(34) Klymchenko, A. S. Fluorescent Probes for Lipid Membranes: From the Cell Surface to Organelles. *Acc. Chem. Res.* **2023**, *56*, 1−12.
(35) Paez-Perez, M.; Kuimova, M. Molecular Rotors: Fluorescent Sensors for Microviscosity and Conformation of Biomolecules. *Angew. Chem., Int. Ed.* **2024**, *63*, No. e202311233.
(36) Wang, L.; Frei, M. S.; Salim, A.; Johnsson, K. Small-Molecule Fluorescent Probes for Live-Cell Super-Resolution Microscopy. *J. Am. Chem. Soc.* **2019**, *141*, 2770−2781.
(37) Grimm, J. B.; Xie, L.; Casler, J. C.; Patel, R.; Tkachuk, A. N.; Falco, N.; Choi, H.; Lippincott-Schwartz, J.; Brown, T. A.; Glick, B. S.; Liu, Z.; Lavis, L. D. A General Method to Improve Fluorophores Using Deuterated Auxochromes. *JACS Au* **2021**, *1*, 690−696.
(38) Wang, J.; Taki, M.; Ohba, Y.; Arita, M.; Yamaguchi, S. Fluorescence Lifetime Imaging of Lipid Heterogeneity in the Inner Mitochondrial Membrane with a Super-Photostable Environment-Sensitive Probe. *Angew. Chem., Int. Ed.* **2024**, *63*, No. e202404328.
(39) Wagner, N.; Stephan, M.; Höglinger, D.; Nadler, A. A Click Cage: Organelle-Specific Uncaging of Lipid Messengers. *Angew. Chem., Int. Ed.* **2018**, *57*, 13339−13343.
(40) Chen, X.-X.; Bayard, F.; Gonzalez-Sanchis, N.; Puji Pamungkas, K. K.; Sakai, N.; Matile, S. Fluorescent Flippers: Small-Molecule Probes to Image Membrane Tension in Living Systems. *Angew. Chem., Int. Ed.* **2023**, *62*, No. e202217868.
(41) Lipsky, N. G.; Pagano, R. E. A Vital Stain for the Golgi Apparatus. *Science* **1985**, *228*, 745−747.
(42) Sawada, S.; Yoshikawa, M.; Tsutsui, K.; Miyazaki, T.; Kano, K.; Mishiro-Sato, E.; Tsukiji, S. Palmitoylation-Dependent Small-Molecule Fluorescent Probes for Live-Cell Golgi Imaging. *ACS Chem. Biol.* **2023**, *18*, 1047−1053.
(43) Erdmann, R. S.; Takakura, H.; Thompson, A. D.; Rivera-Molina, F.; Allgeyer, E. S.; Bewersdorf, J.; Toomre, D.; Schepartz, A. Super-Resolution Imaging of the Golgi in Live Cells with a Bioorthogonal Ceramide Probe. *Angew. Chem., Int. Ed.* **2014**, *53*, 10242−10246.
(44) Wang, H.; Zhang, X.; Xiu, T.; Wang, H.; Li, P.; Tang, B. Fluorescence Probes for Sensing and Imaging within Golgi Apparatus. *Coord. Chem. Rev.* **2024**, *502*, No. 215618.
(45) Liu, C.; Zhu, H.; Zhang, Y.; Su, M.; Liu, M.; Zhang, X.; Wang, X.; Rong, X.; Wang, K.; Li, X.; Zhu, B. Recent Advances in Golgi-Targeted Small-Molecule Fluorescent Probes. *Coord. Chem. Rev.* **2022**, *462*, No. 214504.
(46) Fan, L.; Wang, X.; Ge, J.; Li, F.; Zhang, C.; Lin, B.; Shuang, S.; Dong, C. A Golgi-Targeted off−on Fluorescent Probe for Real-Time

https://doi.org/10.1021/jacsau.4c00487
JACS Au 2024, 4, 3759−3765

Monitoring of pH Changes in Vivo. *Chem. Commun.* **2019**, *55*, 6685−6688.
(47) Jung, K. H.; Oh, E.-T.; Park, H. J.; Lee, K.-H. Development of New Peptide-Based Receptor of Fluorescent Probe with Femtomolar Affinity for Cu+ and Detection of Cu+ in Golgi Apparatus. *Biosens. Bioelectron.* **2016**, *85*, 437−444.
(48) Li, R. S.; Gao, P. F.; Zhang, H. Z.; Zheng, L. L.; Li, C. M.; Wang, J.; Li, Y. F.; Liu, F.; Li, N.; Huang, C. Z. Chiral Nanoprobes for Targeting and Long-Term Imaging of the Golgi Apparatus. *Chem. Sci.* **2017**, *8*, 6829−6835.
(49) Tan, W.; Zhang, Q.; Quiñones-Frías, M. C.; Hsu, A. Y.; Zhang, Y.; Rodal, A.; Hong, P.; Luo, H. R.; Xu, B. Enzyme-Responsive Peptide Thioesters for Targeting Golgi Apparatus. *J. Am. Chem. Soc.* **2022**, *144*, 6709−6713.
(50) Zhang, W.; Zhang, J.; Li, P.; Liu, J.; Su, D.; Tang, B. Two-Photon Fluorescence Imaging Reveals a Golgi Apparatus Superoxide Anion-Mediated Hepatic Ischaemia-Reperfusion Signalling Pathway. *Chem. Sci.* **2019**, *10*, 879−883.
(51) Fang, L.; Crespo-Otero, R.; Jones, C. R.; Watkinson, M. Protect to Detect: A Golgi Apparatus Targeted Probe to Image Mobile Zinc through the Use of a Lipophilic Cell-Labile Protecting Group Strategy. *Sens. Actuators B Chem.* **2021**, *338*, No. 129850.
(52) Li, R. S.; Liu, J.; Shi, H.; Hu, P. P.; Wang, Y.; Gao, P. F.; Wang, J.; Jia, M.; Li, H.; Li, Y. F.; Mao, C.; Li, N.; Huang, C. Z. Transformable Helical Self-Assembly for Cancerous Golgi Apparatus Disruption. *Nano Lett.* **2021**, *21*, 8455−8465.
(53) Tan, W.; Zhang, Q.; Wang, J.; Yi, M.; He, H.; Xu, B. Enzymatic Assemblies of Thiophosphopeptides Instantly Target Golgi Apparatus and Selectively Kill Cancer Cells. *Angew. Chem., Int. Ed.* **2021**, *60*, 12796−12801.
(54) Tan, W.; Zhang, Q.; Hong, P.; Xu, B. A Self-Assembling Probe for Imaging the States of Golgi Apparatus in Live Single Cells. *Bioconjugate Chem.* **2022**, *33*, 1983−1988.
(55) Koide, Y.; Urano, Y.; Hanaoka, K.; Piao, W.; Kusakabe, M.; Saito, N.; Terai, T.; Okabe, T.; Nagano, T. Development of NIR Fluorescent Dyes Based on Si−Rhodamine for in Vivo Imaging. *J. Am. Chem. Soc.* **2012**, *134*, 5029−5031.
(56) Ohno, H.; Sasaki, E.; Yamada, S.; Hanaoka, K. Recent Advances in Si-Rhodamine-Based Fluorescent Probes for Live-Cell Imaging. *Org. Biomol. Chem.* **2024**, *22*, 3099−3108.
(57) Wang, L.; Tran, M.; D'Este, E.; Roberti, J.; Koch, B.; Xue, L.; Johnsson, K. A General Strategy to Develop Cell Permeable and Fluorogenic Probes for Multicolour Nanoscopy. *Nat. Chem.* **2020**, *12*, 165−172.
(58) Nakamura, N.; Rabouille, C.; Watson, R.; Nilsson, T.; Hui, N.; Slusarewicz, P.; Kreis, T. E.; Warren, G. Characterization of a Cis-Golgi Matrix Protein, GM130. *J. Cell Biol.* **1995**, *131*, 1715−1726.
(59) Huang, B.; Li, X.; Zhu, X. The Role of GM130 in Nervous System Diseases. *Front. Neurol.* **2021**, *12*, No. 743787.
(60) Lujan, P.; Garcia-Cabau, C.; Wakana, Y.; Vera Lillo, J.; Rodilla-Ramírez, C.; Sugiura, H.; Malhotra, V.; Salvatella, X.; Garcia-Parajo, M. F.; Campelo, F. Sorting of Secretory Proteins at the Trans-Golgi Network by Human TGN46. *eLife* **2024**, *12*, No. RP91708.
(61) Wakana, Y.; van Galen, J.; Meissner, F.; Scarpa, M.; Polishchuk, R. S.; Mann, M.; Malhotra, V. A New Class of Carriers That Transport Selective Cargo from the Trans Golgi Network to the Cell Surface. *EMBO J.* **2012**, *31*, 3976−3990.
(62) Xie, S.; Bahl, K.; Reinecke, J. B.; Hammond, G. R. V.; Naslavsky, N.; Caplan, S. The Endocytic Recycling Compartment Maintains Cargo Segregation Acquired upon Exit from the Sorting Endosome. *Mol. Biol. Cell* **2016**, *27*, 108−126.
(63) Wong-Dilworth, L.; Rodilla-Ramirez, C.; Fox, E.; Restel, S. D.; Stockhammer, A.; Adarska, P.; Bottanelli, F. STED Imaging of Endogenously Tagged ARF GTPases Reveals Their Distinct Nano-scale Localizations. *J. Cell Biol.* **2023**, *222*, No. e202205107.
(64) Sciaky, N.; Presley, J.; Smith, C.; Zaal, K. J. M.; Cole, N.; Moreira, J. E.; Terasaki, M.; Siggia, E.; Lippincott-Schwartz, J. Golgi Tubule Traffic and the Effects of Brefeldin A Visualized in Living Cells. *J. Cell Biol.* **1997**, *139*, 1137−1155.
(65) Patterson, S. I.; Pate Skene, J. H. Inhibition of Dynamic Protein Palmitoylation in Intact Cells with Tunicamycin. *Methods Enzymol.* **1995**, *250*, 284−300.
(66) Lawrence, D. S.; Zilfou, J. T.; Smith, C. D. Structure−Activity Studies of Cerulenin Analogues as Protein Palmitoylation Inhibitors. *J. Med. Chem.* **1999**, *42*, 4932−4941.
(67) Bayard, F.; Matile, S. Fluorescent Membrane Probes Obey the Israelachvili Rules. *Helv. Chim. Acta* **2024**, *107*, No. e202400062.
(68) Sakai, N.; Assies, L.; Matile, S. G-Quartets, 4-Way Junctions and Triple Helices but Not DNA Duplexes: Planarization of Twisted Push−Pull Flipper Probes by Surface Recognition Rather Than Physical Compression. *Helv. Chim. Acta* **2022**, *105*, No. e202200052.
(69) García-Calvo, J.; López-Andarias, J.; Sakai, N.; Matile, S. Planarizable Push-Pull Probes with Sulfoximine-Bridged Dithienothiophene Acceptors. *Helv. Chim. Acta* **2022**, *105*, No. e202100238.
(70) Fin, A.; Vargas Jentzsch, A.; Sakai, N.; Matile, S. Oligothiophene Amphiphiles as Planarizable and Polarizable Fluorescent Membrane Probes. *Angew. Chem., Int. Ed.* **2012**, *51*, 12736−12739.
(71) Digman, M. A.; Caiolfa, V. R.; Zamai, M.; Gratton, E. The Phasor Approach to Fluorescence Lifetime Imaging Analysis. *Biophys. J.* **2008**, *94*, L14−L16.
(72) Rahim, M. K.; Zhao, J.; Patel, H. V.; Lagouros, H. A.; Kota, R.; Fernandez, I.; Gratton, E.; Haun, J. B. Phasor Analysis of Fluorescence Lifetime Enables Quantitative Multiplexed Molecular Imaging of Three Probes. *Anal. Chem.* **2022**, *94*, 14185−14194.
(73) Pamungkas, K. K. P.; Fureraj, I.; Assies, L.; Sakai, N.; Mercier, V.; Chen, X.-X.; Vauthey, E.; Matile, S. Core-Alkynylated Fluorescent Flippers: Altered Ultrafast Photophysics to Track Thick Membranes. *Angew. Chem., Int. Ed.* **2024**, *63*, No. e202406204.
(74) Bayard, F.; Chen, X.-X.; García-Arcos, J. M.; Roux, A.; Sakai, N.; Matile, S. Hydrophobic Interfacing of Fluorescent Membrane Probes. *ChemistryEurope* **2023**, *1*, No. e202300041.
(75) López-Andarias, J.; Eblighatian, K.; Pasquer, Q. T. L.; Assies, L.; Sakai, N.; Hoogendoorn, S.; Matile, S. Photocleavable Fluorescent Membrane Tension Probes: Fast Release with Spatiotemporal Control in Inner Leaflets of Plasma Membrane, Nuclear Envelope, and Secretory Pathway. *Angew. Chem., Int. Ed.* **2022**, *61*, No. e202113163.
(76) Straková, K.; López-Andarias, J.; Jiménez-Rojo, N.; Chambers, J. E.; Marciniak, S. J.; Riezman, H.; Sakai, N.; Matile, S. HaloFlippers: A General Tool for the Fluorescence Imaging of Precisely Localized Membrane Tension Changes in Living Cells. *ACS Cent. Sci.* **2020**, *6*, 1376−1385.
(77) Chen, X.-X.; Gomila, R. M.; García-Arcos, J. M.; Vonesch, M.; Gonzalez-Sanchis, N.; Roux, A.; Frontera, A.; Sakai, N.; Matile, S. Fluorogenic In Situ Thioacetalization: Expanding the Chemical Space of Fluorescent Probes, Including Unorthodox, Bifurcated, and Mechanosensitive Chalcogen Bonds. *JACS Au* **2023**, *3*, 2557−2565.
(78) Lista, M.; Areephong, J.; Sakai, N.; Matile, S. Lateral Self-Sorting on Surfaces: A Practical Approach to Double-Channel Photosystems. *J. Am. Chem. Soc.* **2011**, *133*, 15228−15231.
(79) Hayashi, H.; Sobczuk, A.; Bolag, A.; Sakai, N.; Matile, S. Antiparallel Three-Component Gradients in Double-Channel Surface Architectures. *Chem. Sci.* **2014**, *5*, 4610−4614.
(80) Zhang, Q.; Qu, D.-H.; Feringa, B. L.; Tian, H. Disulfide-Mediated Reversible Polymerization toward Intrinsically Dynamic Smart Materials. *J. Am. Chem. Soc.* **2022**, *144*, 2022−2033.
(81) Fabre, B.; Pícha, J.; Vaněk, V.; Selicharová, I.; Chrudinová, M.; Collinsová, M.; Žáková, L.; Buděšínský, M.; Jiráček, J. Synthesis and Evaluation of a Library of Trifunctional Scaffold-Derived Compounds as Modulators of the Insulin Receptor. *ACS Comb. Sci.* **2016**, *18*, 710−722.

https://doi.org/10.1021/jacsau.4c00487
JACS Au 2024, 4, 3759−3765